J. Appl. Comput. Mech., 12(3) (2026) 1035-1046
DOI: 10.22055/jacm.2025.48830.5529

ISSN: 2383-4536
jacm.scu.ac.ir

Shahid Chamran University of Ahvaz

Journal of Applied and Computational Mechanics

Research Paper

Central Composite Design-Based Parametric Study of Magnetically Dissipative Darcy–Forchheimer Hybrid Nanofluid Flow over an Expanding Sheet

Rajat Srivastava[1], Ram Prakash Sharma[2]

[1] Department of Basic & Applied Science, National Institute of Technology Arunachal Pradesh, Jote, Papum Pare District, Arunachal Pradesh-791113, India, Email: rajat.phd20@nitap.ac.in

[2] Department of Mechanical Engineering, National Institute of Technology Arunachal Pradesh, Jote, Papum Pare District, Arunachal Pradesh-791113, India, Email: rpsharma@nitap.ac.in

Received October 14 2025; Revised November 16 2025; Accepted for publication December 04 2025.
Corresponding author: R.P. Sharma (rpsharma@nitap.ac.in)

Abstract. This study investigates the effect of magnetic interactions on two-dimensional electrically conducting hybrid nanofluid flow over an expanding sheet, considering porous media and Darcy forces. In addition, the study addresses the role of Ohmic and Joule heating effects on the heat transfer processes of a copper–alumina hybrid nanofluid suspended in water. Here, Mintsa model is applied to control thermal conductivity whereas Gharesim model is applied to ascertain viscosity. Using similarity transformations, the governing conservation equations for fluid flow are converted into nonlinear ordinary differential equations. The application of the Runge–Kutta 4–5th order approach enables accurate and efficient numerical resolution of the governing system. In addition, the Response Surface Method (RSM), a robust statistical approach, is utilized to investigate the enhancement of heat transfer across multiple parameters, where optimal findings are validated through Analysis of Variance (ANOVA). The paper shows a high level of congruence with previous studies in certain instances and gives the physical meaning of the added parameters through graphs and table. Graphical representations demonstrate that augmented magnetic field strength elevated the fluid temperature of the nanofluid, resulting in heightened surface friction and thermal transfer rate. However, when the intensity of the magnetic field intensified, there was a corresponding decrease in the rate of heat transfer until a specific threshold was reached. This investigation has practical applications in improving the heat managing systems. The renewable energy management, cooling effects in electronic devices, and trade heat exchangers, by refining heat transmission efficacy and fluid performance.

Keywords: Hybrid nanofluid; Magnetic field; Porous media; Viscous dissipation; Response surface methodology.

1. Introduction

Recent research has introduced nanofluids, which are colloidal solutions containing nanoparticles that greatly improve thermal conductivity. Their importance has grown rapidly, making it necessary to study their applications in different areas. Nanofluids are now being used in transportation, refrigeration, air conditioning, microelectronics, fuel cells, solar heating, medicine, drug delivery, mobile processors, and even military communication systems. Many researchers have explored these and its other potential applications. Raza et al. [1] examined the hybrid nanofluid flow and heat transfer characteristics across porous surfaces. Abbas et al. [2] investigated the flow of radiated Casson hybrid nanofluid across a surface with Soret and Dufour effects. Feng et al. [3] conducted experimental research on nano-organic fluids containing surfactants, revealing higher stability, improved heat transfer, and diminished pressure drops in Organic Rankine Cycle systems. Raza et al. [4] explored the ternary nanofluid flow with nanoparticle shape effects over a rotating porous walls associated with permeable Reynolds numbers. Jaiswal et al. [5] examined micropolar fluid dynamics in an anisotropic porous channel with slip boundaries, demonstrating diminished entropy generation and implications for heat exchangers, microfluidics, and solar collectors. Raza et al. [6] examined the bioconvective nanofluid flow phenomena and thermal exploration passing through two orthogonal permeable porous discs. Nourmohammadi et al. [7] analysed nanofluid applications aimed at boosting the effectiveness of thermal treatment in pomegranate juice processing.

The goal has been to comprehend and enhance the thermal characteristics of nanofluids ever since they were first introduced. Traditionally, just one nanoparticle makes up traditional nanofluids. Hybrid nanofluids have been created to overcome these drawbacks. Nanoparticles of more than one types are present in these fluids. Ashwinkumar et al. [8] focused on hybrid nanofluid flow behavior over two geometrical setups to determine heat transfer rates under magnetic and thermal radiation conditions. A radial porous fin fully immersed in fluid and experiencing convective–radiative heat transfer was studied by Keerthi et al. [9], with hybrid nanofluid flowing past it. Thirumalaisamy et al. [10] explored hybrid nanofluid heat transfer performance in a square porous domain. The mathematical model has been addressed using the marker-and-cell numerical methods, and a comprehensive parametric analysis has been conducted. Basha et al. [11] conducted research on hybrid nanofluid flow across three fin shapes to

Published online: December 12 2025

examine thermal performance and compare results for system optimization. Kumar et al. [12] illustrated the hybrid nanofluid flow through the fluid dynamics of a porous cylinder subjected to stretching, heat sources, and chemical interactions. Sharma et al. [13] focused on predicting thermal transfer rate in hybrid nanofluid flow within a porous coaxial disk, influenced by thermal radiation and a low-frequency oscillating magnetic field. Pattnaik et al. [14] explored the importance of hybrid nanoliquid in rocket nozzle cooling research.

The phenomenon of magnetic field interaction in the flow of fluids in enclosures is a topic of growing interest among researchers, and they have immense potential to develop within a wide range of industrial and technological applications. This interest prevails because thousands of untested applications exist out there particularly in advanced manufacturing operations and engineering developments. Magnetic-fluid phenomena are being associated by the scientific community with new opportunities in renewable energy, medicine and aeronautics. As a result, the urgency of research increases to learn the possibilities of magnetic fields in order to cope with the multifaceted issues of contemporary society. Sharma and Srivastava [15] examined fluid dynamics around a rotating sphere under the influence of an applied magnetic field. The effects of magnetic field on fluid motion enclosing a spherical solid under porous constraints were examined by Maurya et al. [16]. Sharma et al. [17] to analyse thermal transport phenomena of fluid flow past a microchannel under magnetic fields. Kumar et al. [18] exemplified a non-classical Stefan problem that involves the space-dependent thermal conductivity. The Genocchi polynomials and the collocation scheme has been utilized to address the mathematical model to illustrate the flow phenomenon. Dolui et al. [19] scrutinized the significance of radiative forces on the hybrid nanoliquid flow via an inclined surface with magnetic field. According to this study, magnetic force governs flow velocity and magnetic field growth, whereas radiation parameter increases the opposite. Raza et al. [20] explored the magnetohydrodynamic (MHD) boundary layer flow of Boger nanofluid over a stretching surface with the influences of nanoparticle diameter and thermal radiation. The thermal transfer rate of nanoliquid stream through a magnetically influenced permeable slider was forecasted using an ANN framework by Kumar et al. [21].

The phenomena of fluid flow through porous media are significant due to its numerous applications in contemporary culture. The impact of thermal transfer and temperature on boundary layer flow in porous media, influenced by a magnetic field, has enhanced thermal performance. A multitude of studies have been undertaken to investigate fluid dynamics in porous media. Usafzai et al. [22] investigated the issue of nanofluid transport in porous media affected by slip and jump phenomena by selecting specific solutions that encompassed stretching or shrinking sheets influenced by differences in velocity slip, permeability, and Prandtl number. Mubaraki et al. [23] studied the chlorine transport in a single-layered pipe and extends it to the case of a bi-layered pipe using a hybrid approach that combines the Laplace transform method as well as asymptotic approximations method. Farooq et al. [24] investigated second-grade MHD nanofluid convection across a porous stretching surface. Ahmed et al. [25] focused on hybrid nanofluid flow over oscillatory curved porous surfaces, demonstrating impact of nanoparticles on heat transfer enhancement and influence periodic behaviors due to curvature and porosity. The significance of magnetic fields in governing nanofluid flow across a rough rotating disk within porous media was investigated by Kumar et al. [26]. Raza et al. [27] deliberated the two-dimensional boundary layer flow and thermal transfer characteristics of incompressible fluid over a plate embedded in a porous medium. Jagadha et al. [28] investigated radiative MHD Casson nanofluid flow through porous media, highlighting how magnetic, thermal, and chemical effects influence velocity reduction and thermal enhancement.

Due to the internal friction of a fluid medium, the generated mechanical energy is converted into heat, which is called viscous dissipation. In the cases of higher viscosity of the fluid motion, the friction among the adjacent layers resists the flow velocity, which raises the temperature of the flow. Sharma and Sharma [29] studied impact of nanoparticle aggregation over a parabolic collector with thermal radiation. Gowtham et al. [30] highlighted the influences of heat source on the third-grade nanoliquid flow past an inclined microchannel. They reported that the increasing Eckert number and external heat source elevate the temperature distribution in a more pronounced way. The interaction of nanoliquid stream amid a fixed elongating disk and a rotating cone was investigated by Madhu et al. [31]. They concluded from the findings that the elevation in the thermophoresis effect accelerates the concentration profile; meanwhile, the augmentation of Brownian motion decelerates it. Additionally, the enhanced Eckert number escalated the temperature dynamics. To escalate the thermal efficacy of the microchannel, Soumya et al. [32] rearranged the energy equation with the Ohmic dissipation and exponential heat source effects. They also analysed the generated entropy of the system. Their findings suggested that the augmenting impact dissipation and heat source increases the Nusselt number, whereas the diminishing entropy enhances the efficiency of the channel. The significance of chemical reactions on viscous fluid flow over a curved surface was analysed by Sharma and Sharma [33]. With the utilization of the RK method, they numerically tackled the solution and to predict the accuracy of the heat and mass transmission, they employed a neural network architecture to the flow model. Shamshuddin et al. [34] investigated the thermal characteristics of ternary nanoliquid considering both viscous and Joule dissipation effects. Executing Adomain decomposition method, the behavior of bi-hybrid nanoliquid flow within a rocket engine nozzle was studied thoroughly by Pattanaik et al. [35]. Executing KKL model, Galal et al. [36] examined the three-dimensional flow of a hybrid nanoliquid that past a vertical channel to investigate the thermal transfer performance under dissipative effects. Moreover, to find the statistical significance of the effect, they utilized RSM to statistically interpret it. Kumar et al. [37] analysed MXene bi-hybrid nanoliquid stream over a permeable slider, demonstrating slider dynamics, magnetic and thermal effects, and Taguchi optimization. Fatima et al. [38] conducted a neural network assessment on the heat transportation of the ternary nanoliquid flow passed within a ciliated microtube.

Response surface methodology (RSM) represents a mathematical–statistical framework designed to model and interpret systems where several factors simultaneously affect a specific response. It enables process optimization through systematic evaluation of the interrelationships between input parameters and the corresponding output. Typically, RSM incorporates design of experiments (DOE) to systematically gather data and applies regression analysis to develop predictive models. It serves as a powerful tool for achieving performance optimization, with broad utility in areas including engineering, manufacturing, and design innovation. Malika and Sonawane [39] estimated the effective thermal conductivity of the nanofluid with different complex parameters using RSM and artificial neural network (ANN) modelling techniques at an optimal nanoparticle mixing ratio. Rana et al. [40] theoretically exemplified the stagnation points of nanofluid flow at spinning spheres under thermal boundary conditions. Sharma and Shaw [41] investigated the impact of radiation and dissipative heat on the flow of Casson fluid past an extending surface. Rehman et al. [42] explored the behaviour of nanofluid flow with chemical reactions and nonlinear mixed convection across a stretched surface with statistical approach. Sharma and Sharma [43] explored the magnetized nanoliquid stream across a nonlinear curved stretching surface for several industrial and engineering applications.

1.1. Research gap

- Previous research hasn't looked into how porous medium resistance (Darcy–Forchheimer drag) and magnetic field effects affect the flow of mixed nanofluids enough. This means that we don't fully understand how inertial and viscous forces work in these kinds of systems.

- Not much is known about how viscous dissipation changes temperature profiles and improves thermal transport in hybrid nanofluids, especially for Al_2O_3–Cu systems based with water.
- Response Surface Methodology (RSM) hasn't been used in many studies to systematically improve and study how different factors affect the performance of hybrid nanofluid heat transfer.

1.2. Research questions

- In what way does the addition of Cu and Al_2O_3 nanoparticles alter the thermal properties and heat transfer efficiency of the hybrid nanofluid?
- What effect does the porous medium's permeability and magnetic have on the motion and behavior of fluid across an expanding surface?
- How do modifications in essential parameters affect the effectiveness and applicability of real-world operations?

1.3. Objective

This research deepens the core understanding of hybrid nanofluid dynamics and establishes a reliable framework for developing nanofluids customized for particular applications. The fusion of RSM and sensitivity analysis offers a comprehensive method for developing optimized hybrid nanofluid formulations, contributing to superior heat transfer behavior in practical applications. This study's main goal is to examine the flow and heat transfer properties of a water-based hybrid nanofluid with Al_2O_3 and Cu nanoparticles across a permeable stretching surface while being affected by both Darcy–Forchheimer porous medium effects and a magnetic field. In order to better represent actual flow behaviour, the research also attempts to include inertial drag and viscous dissipation in the governing framework. However, this investigation has practical applications in improving the heat managing systems. The renewable energy management, cooling effects in electronic devices, and trade heat exchangers, by refining heat transmission efficacy and fluid performance.

1.4. Novelty

- To illustrate the flow dynamics of a water-based hybrid nanoliquid enriched with Al_2O_3 and Cu nanoparticles.
- To present the motion and thermal behavior of a water-based hybrid nanofluid with Al_2O_3 and Cu nanoparticles.
- The research focuses on the behavior of hybrid nanofluid flow with Darcy–Forchheimer resistance in the presence of a magnetic field over a permeable stretching surface.
- The innovation of the study lies in the inclusion of the Darcy-Forchheimer framework to reflect inertial drag as well as the influence of viscous dissipation in the intensification of the flow dynamics.
- To examine the improvement in thermal transfer rate for different influencing parameters the RSM is applied.

2. Formulation of the Problem

The 2-D motion of an electrically conducting, MHD, viscous, steady hybrid nanofluid that is flowing over an expanding sheet and contains porous media and Darcy force while considering the impacts of Joule heating and Ohmic dissipation on the heat transference phenomenon of the *Cu-Al_2O_3-water* hybrid nanofluid. The direction of motion of the sheet is perpendicular to the x-axis, which is chosen to be on the y-axis. The wall shown in Fig. 1 is impenetrable (with $v_w = 0$).

- The flow is stable, laminar, and 2D with negligible pressure gradient effects.
- The hybrid nanofluid is considered incompressible with uniform nanoparticle distribution and the base fluid.
- Joule dissipation and magnetic field effects are included.
- The porous medium is modelled using the Darcy–Forchheimer approach to account for both viscous and inertial drag effects.
- The no-slip and initial temperature are considered as the wall temperature at the extending surface. The momentum and temperature asymptotically go to the ambient values.

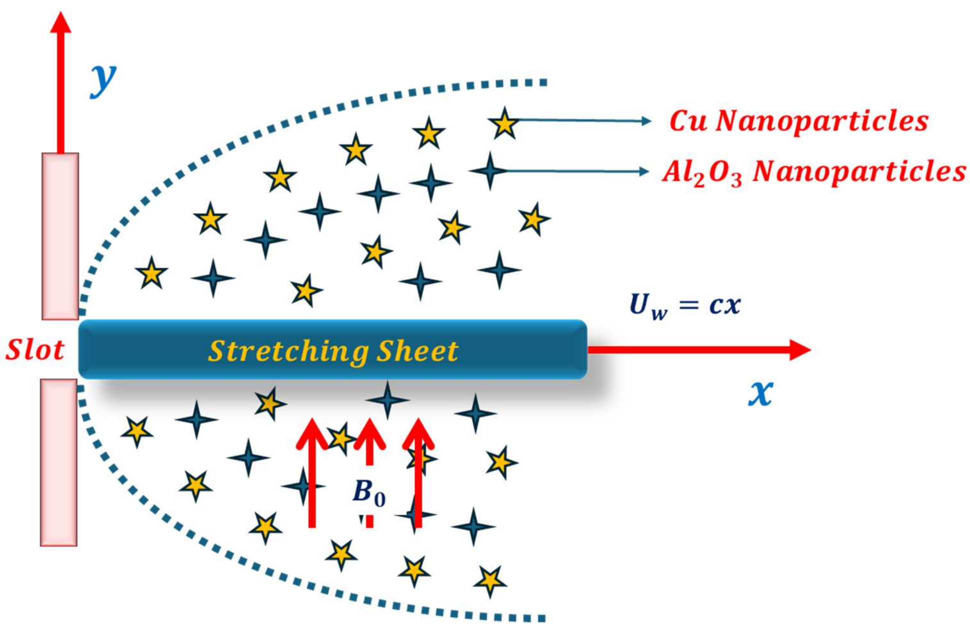

Fig. 1. Flow diagram.

Under the outlined conditions, the equations describing steady boundary layer flow of hybrid nanofluids are formulated as:

$$(v)_y = -(u)_x \tag{1}$$

$$(u)_x \cdot u + (u)_y \cdot v = \nu_{hnf} \cdot (u)_{yy} - \frac{\sigma_{hnf} B^2}{\rho_{hnf}} \cdot u - \frac{\nu_{hnf}}{Kp^*} \cdot u - \frac{C_b}{\rho_{hnf}\sqrt{Kp^*}} \cdot u^2 \tag{2}$$

$$(\rho C_p)_{hnf} \cdot \left(v \cdot (T)_y + u \cdot (T)_x\right) = k_{hnf} \cdot (T)_{yy} + \sigma_{hnf} \cdot B^2 \cdot u^2 + \frac{\mu_{hnf}}{Kp^*} \cdot u^2 \tag{3}$$

The flow configuration adheres to the following boundary conditions:

$$\left.\begin{array}{l} U_w = u(0) = c \cdot x,\ u(\infty) = v(0) = 0, \\ T(0) = T_w\ ,\ T(\infty) = T_\infty. \end{array}\right\} \tag{4}$$

2.1. Similarity transformations

The similarity variables used to solve Eqs. (1) to (4) are chosen as:

$$\eta = \left(\frac{c}{\nu_f}\right)^{1/2} \cdot y,\ u = f'(\eta) \cdot c \cdot x,\ v = -f(\eta) \cdot (c \cdot \nu_f)^{\frac{1}{2}},\ \theta \cdot (T_w - T_\infty) = (T - T_\infty), \tag{5}$$

Applying the similarity transformations (5) to Eqs. (2) and (3) converts the boundary-condition-based nonlinear PDEs into the corresponding nonlinear ODEs:

$$\frac{\mu_{hnf}}{\mu_f} \cdot (f)_{\eta\eta\eta} + \frac{\rho_{hnf}}{\rho_f} \cdot \left((f^2)_\eta - f \cdot (f)_{\eta\eta}\right) - \left(M \cdot \frac{\sigma_{hnf}}{\sigma_f} + \frac{\mu_{hnf}}{\mu_f} \cdot Da\right) \cdot (f)_\eta - \frac{\rho_{hnf}}{\rho_f} \cdot Fr \cdot (f^2)_\eta = 0 \tag{6}$$

$$\frac{k_{hnf}}{k_f} \cdot (\theta)_{\eta\eta} + \left(\Pr \cdot \frac{(\rho c_p)_{hnf}}{(\rho c_p)_f} (\theta)_\eta \cdot f + \Pr \cdot \left(\frac{\sigma_{hnf}}{\sigma_f} \cdot M + \frac{\mu_{hnf}}{\mu_f} \cdot Da\right) Ec \cdot (f^2)_\eta\right) = 0 \tag{7}$$

The governing boundary conditions in their transformed state are defined as:

$$\left.\begin{array}{l} f(0) = 0, f'(0) = 1,\ f'(\infty) = 0 \\ \theta(0) = 1, \theta(\infty) = 0. \end{array}\right\} \tag{8}$$

The dimensionless parameters are as follows: Prandtl number $\Pr = \mu_f \cdot (c_p)_f / k_f$, Magnetic field parameter $M = \sigma_f \cdot B_0^2 / (c \cdot \rho_f)$, Forchheimer Parameter $Fr = C_b \cdot x / \sqrt{Kp^*}$, Eckert number $Ec = u_w{}^2 / [(c_p)_f \cdot (T_w - T_\infty)]$, Porosity parameter $Da = \nu_f / (c \cdot Kp^*)$.

The main physical quantities considered, namely the skin friction coefficient and Nusselt number, are defined as follows:

$$C_f = \frac{\mu_{hnf}\left((u)_y\right)_{y=0}}{\rho_f \cdot u_w^2},\ Nu_x = -\frac{x k_{hnf}\left((T)_y\right)_{y=0}}{k_f \cdot (T_w - T_\infty)}$$

Hence,

$$C_{fx} \cdot \mathrm{Re}_x^{1/2} = \frac{(f)_{\eta\eta}(0)}{(1-\phi_1)^{2.5} \cdot (1-\phi_2)^{2.5}},\ Nu_x \cdot \mathrm{Re}_x^{-1/2} = -\frac{k_{hnf}}{k_f} \cdot (\theta)_\eta (0) \tag{9}$$

Table 1. Physical and thermal properties of nanofluid and hybrid nanoliquid systems.

Thermophysical properties	Hybrid nanofluid	Nanofluid
Density	$\frac{\rho_{hnf}}{\rho_f} = (1-\phi_2)\left\{\phi_1 \frac{\rho_{s1}}{\rho_f} + (1-\phi_1)\right\} + \phi_2 \frac{\rho_{s2}}{\rho_f}$	$\rho_{nf} = (1-\phi_1)\rho_f + \phi_1 \rho_{s1}$
Dynamic viscosity (Mintsa model [6])	$\frac{\mu_{hnf}}{\mu_f} = \{(1-\phi_2)(1-\phi_1)\}^{-2.5}$	$\mu_{nf} = \mu_f (1-\phi_1)^{-2.5}$
Heat capacity	$\frac{(\rho c_p)_{hnf}}{(\rho c_p)_f} = [\phi_1 \frac{(\rho c_p)_{s1}}{(\rho c_p)_f} + (1-\phi_1)](1-\phi_2) + \phi_2 \frac{(\rho c_p)_{s2}}{(\rho c_p)_f}$	$\frac{(\rho c_p)_{nf}}{(\rho c_p)_f} = (1-\phi_1) + \phi_1 \frac{(\rho c_p)_{s1}}{(\rho c_p)_f}$
Thermal conductivity (Gharesim model [4])	$\frac{k_{hnf}}{k_{nf}} = \frac{2k_{nf} + k_{s2} - 2\phi_2(k_{nf} - k_{s2})}{2k_{nf} + k_{s2} + \phi_2(k_{nf} - k_{s2})}$	$\frac{k_{nf}}{k_f} = \frac{2k_f + k_{s1} - 2\phi_1(k_f - k_{s1})}{2k_f + k_{s1} + \phi_1(k_f - k_{s1})}$
Electrical conductivity	$\frac{\sigma_{hnf}}{\sigma_{nf}} = \frac{\sigma_{s2} + 2\sigma_{nf} + 2\phi_2(\sigma_{s2} - \sigma_{nf})}{\sigma_{s2} + 2\sigma_{nf} - \phi_2(\sigma_{s2} - \sigma_{nf})}$	$\frac{\sigma_{nf}}{\sigma_f} = \frac{\sigma_{s1} + 2\sigma_f + 2\phi_1(\sigma_{s1} - \sigma_f)}{\sigma_{s1} + 2\sigma_f - \phi_1(\sigma_{s1} - \sigma_f)}$

Table 2. Thermo-physical characteristics of fluid and nanoparticles (Abdelmalek et al. [47] and Raza et al. [48]).

Properties	$\rho(kg/m^3)$	$c_p(j/kgK)$	$k(W/mK)$	$\sigma(s/m)$
Fluid phase-water	997.1	4180.0	0.6130	59.6×10^6
Al_2O_3	3970.0	765.0	40.00	35×10^6
Cu	8933.0	385.0	401.0	$\times 10^{-6}$

Table 3. Verification of the outcome for certain Prandtl numbers.

Pr	Devi and Devi [45]	Khan and Pop [44]	Present
2	0.91135	0.9113	0.8882133
6.13	1.75968	----	1.7363614
7	1.8954	1.8954	1.87211
20	3.3539	3.3539	3.3308567

3. Model and Thermo-Physical Properties

To analyze the boundary layer equations of a hybrid nanofluid, this research proposes a novel thermophysical property. Hybrid nanofluid is created by mixing $Cu\ (\phi_1)$ nanoparticles with different solid volume fractions in 0.1vol. of solid volume fractions of $Al_2O_3\ (\varphi_2)$ nanoparticles mixed with water to create the necessary hybrid nanofluid referred to as $Cu/Al_2O_3-water$. Ultimately Table 1 shows the effectual thermophysical characteristics of spherical nanoparticles for nanofluid and hybrid nanofluid to make it obvious. The fundamental thermophysical characteristics of nanofluids are obtained from mainstream works of literature. Table 2 shows the effectual thermophysical characteristics of the fluid phase- water and alumina and copper nanoparticles at 25°C.

4. Computational Solution

The Ohmic dissipation of a hybrid nanofluid flow with electrical conductivity across an expanding surface is examined in this article. By considering the effects of porous media and dissipative heat energy resulting from magnetic field interaction, the heat transport process is improved. By adding metal nanoparticles Cu and oxide nanoparticles Al_2O_3 to the base liquid water, the thermal and physical characteristics of the hybrid nanofluid are illustrated. The temperature dispersal and, consequently, the fluid's thermal conductivity would be impacted by the addition of Joule heating and Ohmic dissipation to the issue. Therefore, characterizing the thermal behavior of the hybrid nanofluid and comprehending the impact of the various parameters, including Joule heating, Ohmic dissipation, porous media, and magnetic effects on the heat transfer process, can be done by combining the Mintsa model for thermal conductivity with other models, for example, the Gharesim model (to describe the viscosity of the fluid). Table 1 summarizes the thermophysical characteristics of the water and the nanoparticles. The study examines the impact of volume concentration and other factors on the operation of the system. Cu and Al_2O_3 has volume concentrations that are represented by ϕ_1 (Cu) and ϕ_2 (Al_2O_3), respectively. For pure fluid, without the presence of magnetic parameters, thermal buoyancy, and Joule heating, Table 3 provides validation and a comparison of the present findings with previous research conducted by Khan and Pop [44] and Devi and Devi [45] in particular cases. The outcomes reveal consistent agreement, confirming that the proposed solution meets the convergence requirements. The combined use of the shooting technique and the 4th RK approach enables accurate computation of boundary value problems by converting them into a series of initial value problems. The iterations are repeated until the results converge within a specified error limit approximately 10^{-6} and maintain a constant step size of 0.001.

5. Analysis of Results and Discussion

The physical significance of the various quantities influencing the flow phenomena of the hybrid nanofluid is shown in Figs. 2 to 11. Here, the concentrations of Al_2O_3 and Cu in the base liquid water are taken to be 0 to 20% and 0 to 15%, respectively. The behavior of the particle concentration on the fluid velocity profile is elaborated in Fig. 2. Interestingly, an increment in Al_2O_3 nanoparticle concentration shows an increase. In contrast, an increase in Cu nanoparticle concentration shows a decrease in the velocity profile. Due to the higher density of Cu, it enhances the agglomeration of particles. So, it enhances the resistance and hence declines the velocity domain. In contrast, adding Al_2O_3 particles decreases the viscosity due to its lower density and lower conductivity compared to Cu, thereby raising fluid movement. The clogging near the surface caused by the density of Cu nanoparticles being much higher than that of Al_2O_3 nanoparticles. Additionally, compared to pure water, the size and shape of Cu nanoparticles exhibit a slightly greater friction factor. This shows that in comparison to Al_2O_3 / water nanofluids, diluted $Cu/Al_2O_3-\text{water}$ hybrid nanofluids will result in a decrease in velocity.

Figure 3 visualizes the influence of nanoparticle concentration on fluid temperature. The fluid temperature is increased by the presence of volume concentration since the particles have enhanced thermal conductivity. The release of stored energy in the surface area results in an elevation of fluid temperature and an expansion of the thickness of the bounding surface. The example of a hybrid nanofluid has the highest rate of growth in comparison to the pure and nanofluid situations. Therefore, the use of hybrid nanofluid is gaining importance in various industries and engineering gadgets for achieving the desired size and form of the product. The response of a conductive liquid to the magnetic field is seen in Fig. 4. The plot represents the impact of the magnetic force on presence or absence of the hybrid nanofluid containing both types of nanoparticles. The introduction of a magnetic force yields a resistive Lorentz force, which acts in opposition to the profile and reduces velocity. The addition of nanoparticles $\phi_{Cu}, \phi_{Al_2O_3} > 0$ boost the thermal conductivity and also boosts the diffusion of momentum. Thus, the velocity declines more than the pure fluid. Figure 5 shows the effect of magnetic parameters on the thermal profile of the fluid in presence/absence of ϕ_{Cu} and $\phi_{Al_2O_3}$. The Lorentz force, which counteracts the fluid's velocity, results in an accumulation of energy near the surface, thereby the temperature of the fluid increases. Both enhanced conductivity by the addition of $\phi_{Cu}, \phi_{Al_2O_3} > 0$ and the resistive force produced by an upsurge in the magnetic parameter contribute to a growth in the fluid temperature. Figure 6 depicts the system behavior varies with the Eckert number, which is a measure of the coupling parameter, and the fluid temperature for both pure fluid and hybrid nanofluid. The Eckert number arises from a consideration of the dissipative heat energy in this system. It is defined mathematically as the inverse of the temperature differential between the plate's surface and the surrounding temperature.

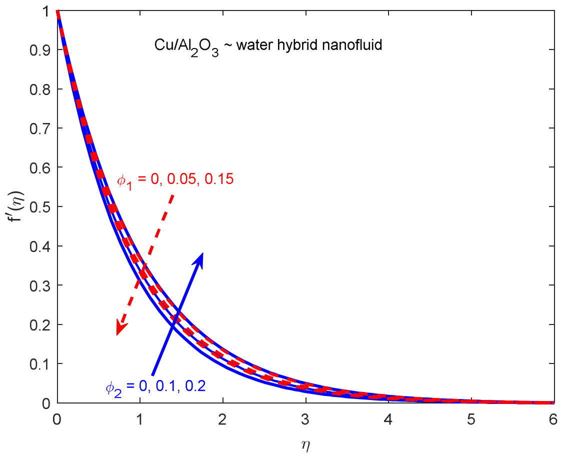

Fig. 2. Variations of ϕ_1 (Cu) and ϕ_2 (Al_2O_3) for $f'(\eta)$.

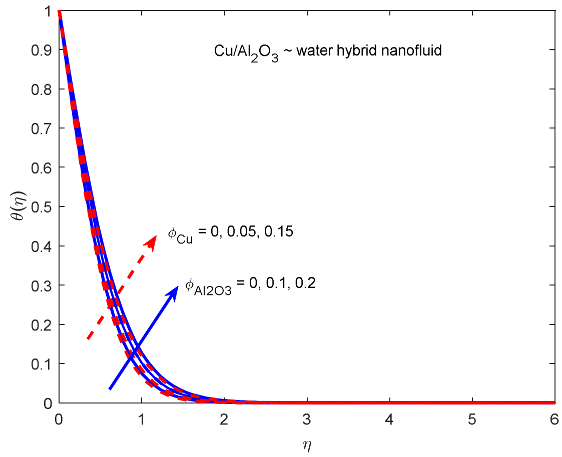

Fig. 3. Variations of ϕ_{Cu} and $\phi_{Al_2O_3}$ for $\theta(\eta)$.

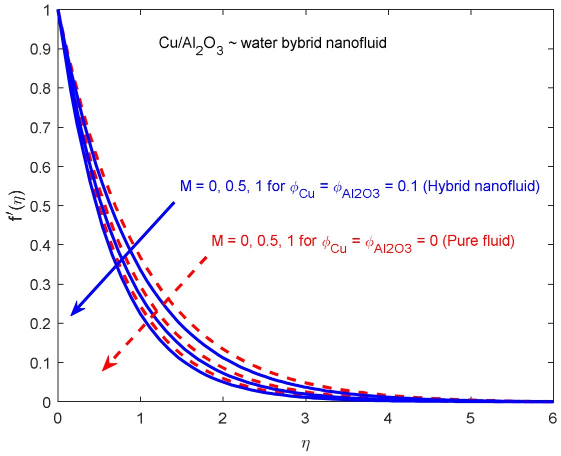

Fig. 4. Variations of parameter M for $f'(\eta)$.

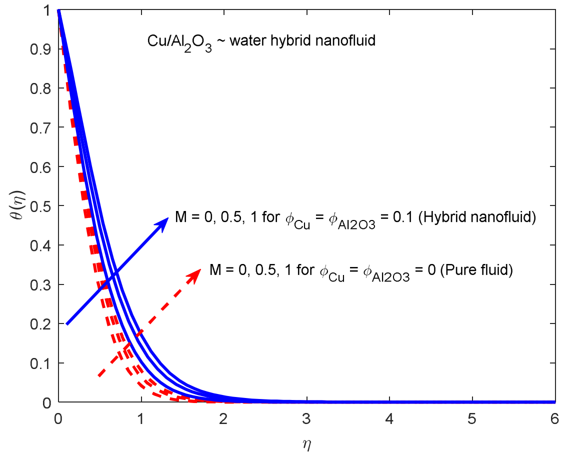

Fig. 5. Variations of parameter M for $\theta(\eta)$.

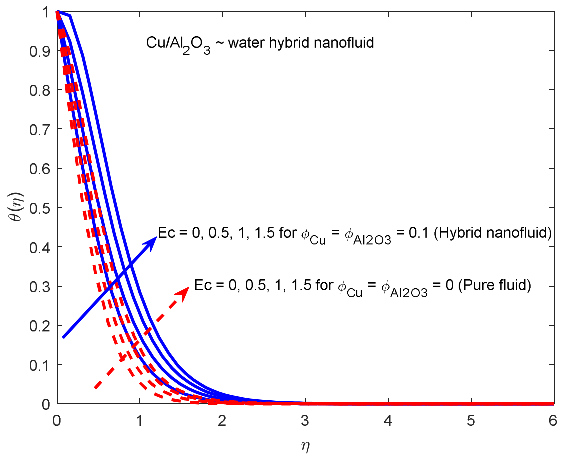

Fig. 6. Variations of parameter Ec for $\theta(\eta)$.

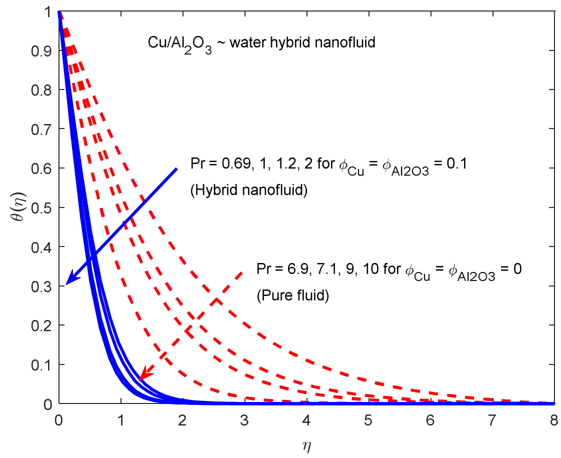

Fig. 7. Variations of parameter Pr for $\theta(\eta)$.

As the Eckert number increases, the profile across the domain also rises. The drag between nanofluid particles causes heat due to viscous dissipation, which elevates the fluid's initial temperature. Figure 7 demonstrates the influence of Pr on the thermal profile of $Cu - Al_2O_3 / H_2O$. A higher Prandtl number reduces the temperature of the nanofluid by decreasing thermal diffusivity. Figures 8 and 9 demonstrate that C_f for Al_2O_3 nanoparticles and Cu nanoparticles rises as for the non-magnetic case $M = 0$, and for magnetic field intensity, respectively. These results suggest that the occurrence of a magnetic field enhances the viscosity of the nanofluid, leading to an increased surface friction force. This force is more pronounced when the volume concentration of Al_2O_3 nanoparticles and Cu nanoparticles is higher. Figures 10 and 11 show that the Nusselt number for Al_2O_3 nanoparticles and Cu nanoparticles exhibit an upward trend as for the non-magnetic case $M = 0$, and the presence of the magnetic field intensity, respectively. The involvement of $\phi_{Cu}, \phi_{Al_2O_3} > 0$ the accelerates the conductivity of nanoparticles, facilitating high thermal transfer via convection. Thus, the rate of thermal energy exchange via convection in the nanoliquid escalates with the augmentation of nanoparticle concentration, leading to a higher Nusselt number. This enhancement in heat transmission is mitigated by the escalating viscosity of the nanofluid.

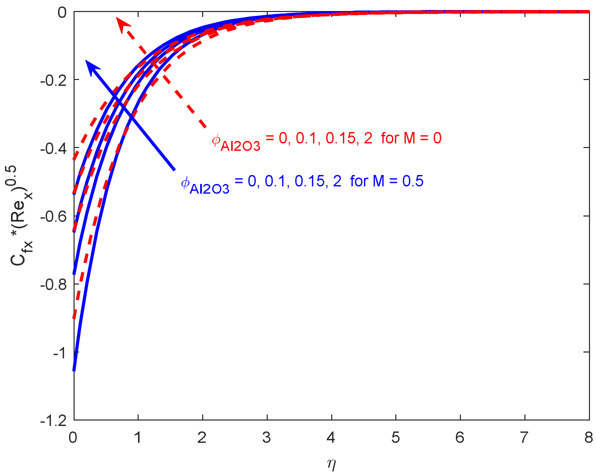

Fig. 8. Variations of C_{fx} for various $\phi_{Al_2O_3}$ values.

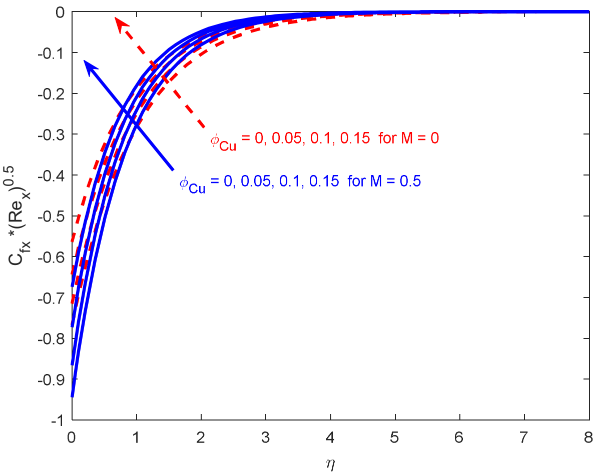

Fig. 9. Behavior of skin friction coefficient for ϕ_{Cu} values.

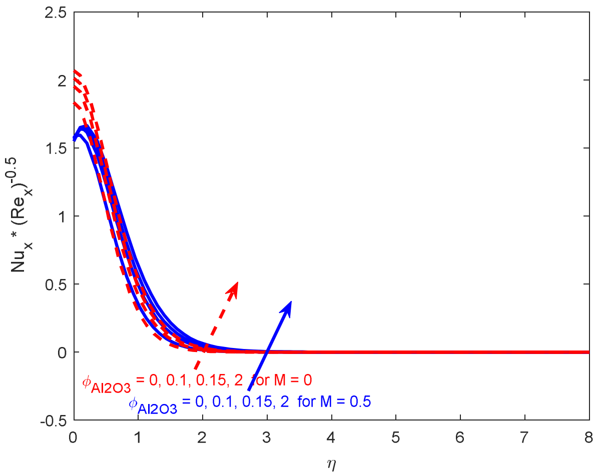

Fig. 10. Behavior of the Nu_x for $\phi_{Al_2O_3}$ values.

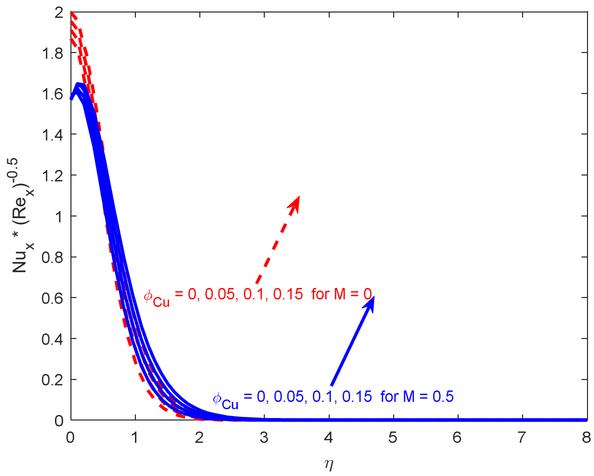

Fig. 11. Behavior of the Nu_x for various ϕ_{Cu} values.

6. Statistical Analysis

Theoretical evaluation of heat transport rate is performed using multiple influencing parameters, and the derived outcomes are regarded as observed heat transfer values. Consequently, a statistical validation is undertaken using RSM to develop a predictive model for the heat transfer rate [49]. The model implementation involves three parameters influencing the Nu_x: Eckart number, Darcy number, and nanoparticle volume fraction. A stepwise RSM procedure for heat transfer prediction is elaborated, with validation carried out through an ANOVA analysis. RSM serves as an advanced optimization and modeling approach that applies integrated mathematical and statistical tools to complex systems. The approach develops intervariable connections to assess the dependency of output performance on multiple input parameters. Owing to its methodological flexibility, RSM finds practical relevance in industries ranging from petrochemical engineering to microbiological process optimization.

6.1. Design of experiments

The predictive model for estimating the heat transfer rate is constructed using the previously defined data, constituting a three-factor model. The central composite design (CCD) procedure involves 20 unique runs, producing 20 predicted Nusselt number values using the RSM approach. Table 4 compiles the CCD results from 20 runs, including 8 cubic, 6 axial, and 6 central experimental points. The analysis also involves estimating standard errors to verify the adequacy of the data fitting process.

To confirm the reliability of the predictive results, an ANOVA test is employed to statistically evaluate the accuracy of the observed Nu_x outcomes. Through this methodology, the heat transfer rate model incorporating three key parameters is mathematically formulated as follows:

$$Nu_x = \Upsilon_1 + \Upsilon_2 A + \Upsilon_3 B + \Upsilon_4 C + \Upsilon_5 A*A + \Upsilon_6 B*B + \Upsilon_7 C*C + \Upsilon_8 A*B + \Upsilon_9 A*C + \Upsilon_{10} B*C, \quad (10)$$

Here, Υ_i (i = 1-10) are identified as the coefficients of the quadratic equation generated through RSM, employed to determine the parametric effects on heat transfer behavior. The summary of the present model is tabulated in Table 5.

6.2. Regression equation in uncoded units

$$\begin{aligned} Nu_x = {} & -2.5603 - 2.27\,\phi_1 + 0.0402\,Da + 3.962\,Ec + 19.6\,\phi_1*\phi_1 - 0.00054\,Da*Da \\ & - 2.419\,Ec*Ec + 0.097\,\phi_1*Da - 0.96\,\phi_1*Ec - 0.0504\,Da*Ec \end{aligned} \quad (11)$$

Table 4. ANOVA table.

Source	DF	Adj SS	Adj MS	F-Value	P-Value
Model	9	2.04499	0.22722	373.07	0.000
Linear	3	1.90417	0.63472	1042.15	0.000
ϕ_1	1	0.00339	0.00339	5.56	0.040
Da	1	0.01908	0.01908	31.32	0.000
Ec	1	1.88170	1.88170	3089.58	0.000
Square	3	0.13750	0.04583	75.26	0.000
$\phi_1 * \phi_1$	1	0.00006	0.00006	0.09	0.769
$Da * Da$	1	0.00007	0.00007	0.11	0.744
$Ec * Ec$	1	0.13496	0.13496	221.59	0.000
2-Way Interaction	3	0.00332	0.00111	1.82	0.208
$\phi_1 * Da$	1	0.00003	0.00003	0.05	0.828
$\phi_1 * Ec$	1	0.00003	0.00003	0.05	0.830
$Da * Ec$	1	0.00326	0.00326	5.35	0.043
Error	10	0.00609	0.00061		
Lack-of-Fit	5	0.00609	0.00122	*	*
Pure Error	5	0.00000	0.00000		
Total	19	2.05108			

Table 5. Overview of the statistical model.

S	R-sq	R-sq (adj)	R-sq (pred)
0.0246789	99.70%	99.44%	97.74%

Figure 12 illustrates the interaction between Da and ϕ_1 on the Nu_x, presented through both contour and surface visualizations. The contour plots map the Nu_x on a two-dimensional plane, taking Da and ϕ_1 as coordinate axes. The interaction between Da and ϕ_1 is evident through the spacing and curvature of the contour lines. The interaction between these parameters produces a noticeable improvement in heat transfer rate. A three-dimensional depiction through surface plotting highlights the Nu_x dependence on both influencing factors. In Fig. 13, the combined effect of ϕ_1 and Ec on heat-transfer response is portrayed via contour surface plots. The contour diagrams link points of identical Nu_x, allowing visual interpretation of variation trends. The degree of contour line proximity reflects the rate of Nu_x variation closer lines correspond to stronger effects. In contrast, the surface plot provides a smooth 3D visualization of Nu_x variation, clarifying the parameter interrelations. Elevated regions on the surface plot denote enhanced heat transfer, while depressions indicate reduced Nu_x. Figure 14 provides a contour visualization showing the interplay between Ec and Da impact on the Nu_x. Each contour delineates a steady-state Nusselt magnitude, providing a layered view of performance variation. The surface plot visualizes the combined effects of Ec and Da dependencies on the Nu_x.

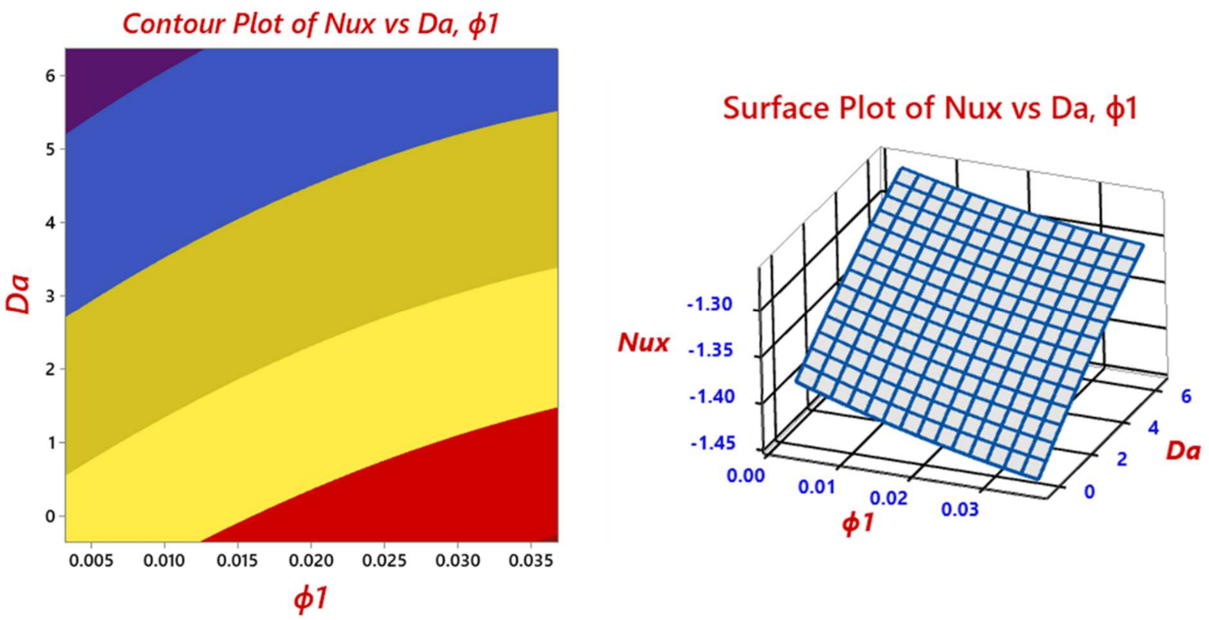

Fig. 12. Contour and surface plots: Da and ϕ_1.

Table 6. Table of sensitivity analysis.

ϕ_1	Ec	$\frac{\partial Nu_x}{\partial \phi_1}$	$\frac{\partial Nu_x}{\partial Ec}$	$\frac{\partial Nu_x}{\partial Da}$
	-1	-5.23	9.760	-0.0064
-1	0	-6.19	4.922	-0.0504
	+1	-7.15	0.084	-0.1072
	-1	-1.31	8.800	0.0906
0	0	-2.27	3.962	0.0402
	+1	-3.23	-0.876	-0.0102
	-1	2.61	7.840	0.1876
+1	0	1.65	3.002	0.1372
	+1	0.69	-1.836	0.0868

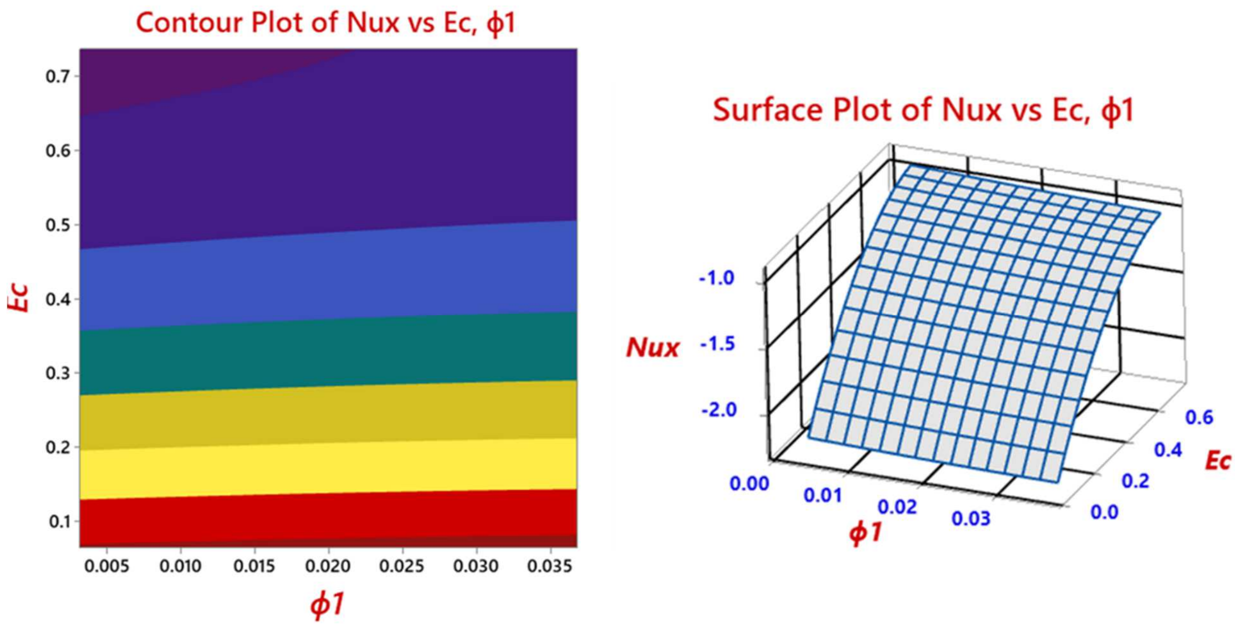

Fig. 13. Contour and surface plots: *Ec* and ϕ_1.

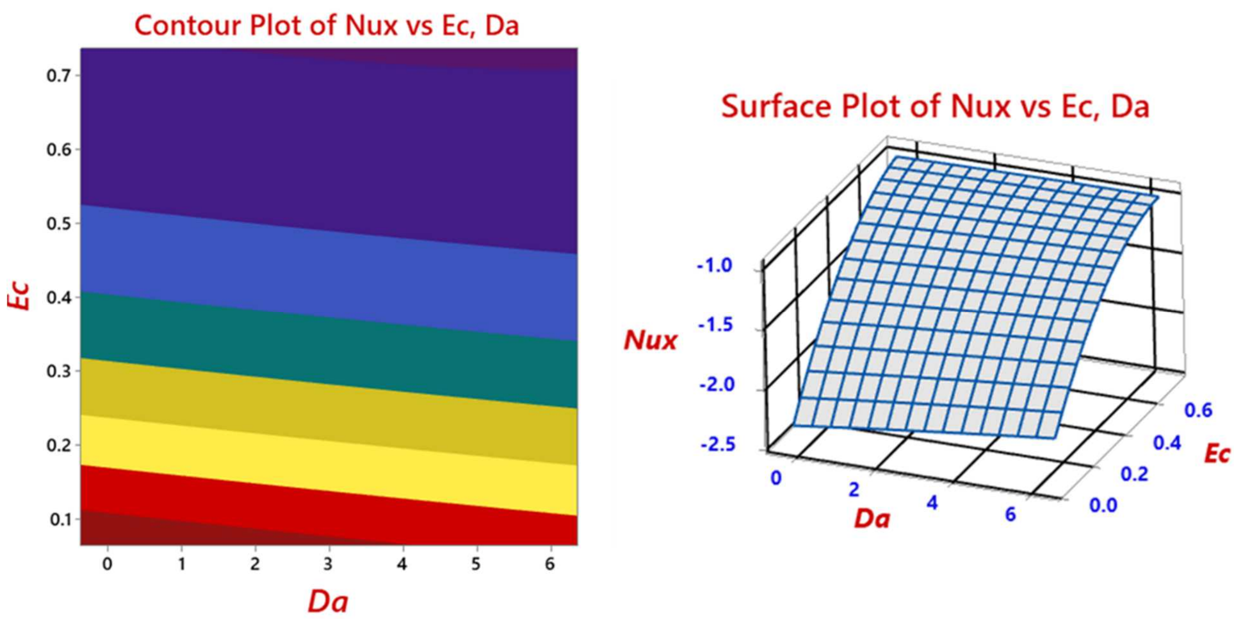

Fig. 14. Contour and surface plots: *Ec* and *Da*.

6.3. Sensitivity analysis

To elaborate the sensitivity of the parameters on the output response, the sensitivity analysis is conducted. This study demonstrates the sensitivity of ϕ_1, Ec, and Da on the Nu_x profile through the partial derivative of Eq. (11). After the derivation, the modified partial derivatives are expressed below:

$$\left.\begin{aligned} \frac{\partial Nu_x}{\partial \phi_1} &= -2.27 + 3.92\phi_1 + 0.097Da - 0.96Ec \\ \frac{\partial Nu_x}{\partial Ec} &= 3.962 - 4.838Ec - 0.96\phi_1 - 0.0504Da \\ \frac{\partial Nu_x}{\partial Da} &= 0.0402 - 0.00108Da + 0.097\phi_1 - 0.0504Ec \end{aligned}\right\} \tag{12}$$

Table 6 illustrates the sensitivity of the above-mentioned parameters on the Nu_x profile. The positive and negative sensitivities represent the increasing and decreasing phenomena of the parameters on the output response.

7. Conclusion

The study researched the influences of varying factors on the stream behavior of hybrid nanofluids and their impacts on heat transfer. The study aims to explore the flow and heat transfer characteristics of a water-based hybrid nanofluid containing Al_2O_3 and Cu nanoparticles. It further examines the effects of Joule heating and Darcy dissipation on the thermal behavior of the Cu–Al_2O_3/water hybrid nanofluid. The following major findings were made:

- The augmentation of Al_2O_3 nanoparticle concentration resulted in a rise in velocity, but the presence of Cu nanoparticles resulted a reduction due to clogging.
- The presence of nanoparticles enhances fluid temperature due to improved thermal conductivity, therefore hybrid nanofluids show the highest temperature increase compared to pure and nanofluid cases.
- The introduction of a magnetic force (Lorentz force) opposed the velocity profile, resulting in diminished velocity with increasing magnetic parameter values, and the absence of magnetic parameters led to maximum velocity results.
- Enhanced magnetic field strength improved the fluid temperature of the nanofluid, leading to increased surface friction and thermal transfer rate. However, as the strength of the magnetic field increased, resulting in a reduction in heat transmission rate until a certain point.
- An increasing Eckert number led to a rise in the profile throughout the domain due to heat generation from viscous dissipation, which elevates the initial temperature of the fluid.
- A higher Prandtl number reduces nanofluid temperature due to decreased thermal diffusivity and boundary layer thickness.
- Using statistical modeling, a predictive design for the Nusselt number is formulated, incorporating the effects of several contributing variables.
- Based on p-values and calculated errors, the quadratic model emerges as the most suitable representation for the Nusselt number.

To summarise, the study's findings illustrate the intricate interaction between several factors affecting the flow and heat transformation properties of hybrid nanofluids. These developments have ramifications for engineering uses, especially in industries where precise control of temperature and fluid flow is crucial. Further research and experimentation are needed to explore the practical applications of these insights. furthermore, the limitation of study incorporates the ideal assumption of nanofluid like uniform dispersion and absence of agglomeration. Also, the application of RSM may not fully define the non-linear interaction outside the selected range of parameter.

Author Contributions

R. Srivastava developed the mathematical modeling, solved the problem and examined the theory validation. R.P. Sharma planned the scheme, initiated the project, and suggested the concept; The manuscript was written through the contribution of all authors. All authors discussed the results, reviewed, and approved the final version of the manuscript.

Acknowledgments

Not applicable.

Conflict of Interest

The authors declared no potential conflicts of interest concerning the research, authorship, and publication of this article.

Funding

The authors received no financial support for the research, authorship, and publication of this article.

Data Availability Statements

The datasets generated and/or analyzed during the current study are available from the corresponding author on reasonable request.

Nomenclature

T	Fluid's temperature (K)	η	Similarity variable
T_w	Wall's temperature (K)	θ	Temperature

T_∞	Temperature far-off from the sheet (K)
u	x -direction's velocity component (m/s)
v	y -direction's velocity component (m/s)
h	Coefficient of Heat transfer (W / (m^2·K))
Cp_f	Fluid's specific heat capacity (J/ (kg · K))
Kp^*	Porosity constant (m^2)
g	The acceleration caused by gravity (m/s^2)
k_f	Fluid's thermal conductivity (W/mK)
μ_f	Fluid's dynamic viscosity (m^2/s)
ν_f	Fluid's kinematic viscosity (m^2/s)
ρ_f	Fluid's density (kg/m^3)
σ	Electrical conductivity (Ω·m)
ρc_p	Heat capacity (J/K)

Dimensionless Parameters

$\phi_{s1} = \phi_1$	Volume fraction of alumina nanoparticle
$\phi_{s2} = \phi_2$	Volume fraction of copper nanoparticle
C_b	Drag coefficient
Pr	Prandtl number
Ec	Eckert number
Fr	Forchheimer Parameter
M	The magnetic parameter
Da	The porosity parameter
Re_x	Local Reynolds number
C_{fx}	Local skin friction coefficient
Nu_x	Local Nusselt number

Subscripts

f	Properties of fluid
nf	Properties of nanofluid
hnf	Properties of hybrid nanofluid
s_1	Properties of solid components of Al_2O_3
s_2	Properties of solid components of Cu

References

[1] Raza, Q., Qureshi, M.Z., Khan, B.A., Hussein, A.K., Ali, B., Shah, N.A., Chung, J.D., Insight into dynamic of mono and hybrid nanofluids subject to binary chemical reaction, activation energy, and magnetic field through the porous surfaces, *Mathematics*, 10, 2022, 3013.

[2] Abbas, M., Abbas, A., Kanwal, H., Gómez-Aguilar, J.F., Torres-Jiménez, J., Significance of chemical reaction and viscous dissipation on magnetized-Marangoni convective flow of dusty Casson hybrid (AA7072+AA7075/sodium alginate) nanofluid with Soret and Dufour effects, *International Journal of Modelling and Simulation*, 2024, 1–18.

[3] Feng, Y., Liu, Z., Xu, K., Wu, H., Wu, Y., Tian, S., Wang, X., Wang, Y., He, Z., Stabilization and heat transfer enhancement of nano-organic fluids in ORC systems: role of surfactant type and concentration in evaporation and condensation processes, *Energy*, 330, 2025, 136849.

[4] Raza, Q., Wang, X., Muhammed, H.A., Ali, B., Ali, M.R., Hendy, A.S., Numerically analyzed of ternary hybrid nanofluids flow of heat and mass transfer subject to various shapes and size factors in two-dimensional rotating porous channel, *Case Studies in Thermal Engineering*, 56, 2024, 104235.

[5] Jaiswal, S., Yadav, N., Yadav, P.K., Sharma, B.D., Entropy generation analysis in unsteady flow of micropolar fluid through anisotropic porous media, *Chinese Journal of Physics*, 2025, https://doi.org/10.1016/j.cjph.2025.07.028.

[6] Raza, Q., Wang, X., Ali, B., Li, S., Shah, N.A., Yang, H., Computational study on entropy generation in Casson nanofluid flow with motile gyrotactic microorganisms using finite difference method, *Chaos, Solitons & Fractals*, 190, 2025, 115758.

[7] Nourmohammadi, A., Ahmadi, E., Jafari, S.M., Nano-fluid thermal processing of pomegranate juice: enhancing efficiency and preserving quality in a shell and tube heat exchanger, *Applied Thermal Engineering*, 274, 2025, 126492.

[8] Ashwinkumar, G.P., Samrat, S.P., Sandeep, N., Convective heat transfer in MHD hybrid nanofluid flow over two different geometries, *International Communications in Heat and Mass Transfer*, 127, 2021, 105563.

[9] Keerthi, M.L., Gireesha, B.J., Sowmya, G., Numerical investigation of efficiency of fully wet porous convective-radiative moving radial fin in the presence of shape-dependent hybrid nanofluid, *International Communications in Heat and Mass Transfer*, 138, 2022, 106341.

[10] Thirumalaisamy, K., Ramachandran, S., Prasad, V.R., Bég, O.A., Leung, H.-H., Kamalov, F., Selvam, R.P., Comparative heat transfer analysis of electroconductive Fe3O4–MWCNT–water and Fe3O4–MWCNT–kerosene hybrid nanofluids in a square porous cavity using the non-Fourier heat flux model, *Physics of Fluids*, 34, 2022, 122016.

[11] Basha, H.T., Sivaraj, R., Jang, B., Entropy analysis and hydrothermal behavior of magnetohydrodynamic MOS2–Fe3O4/H2O hybrid nanofluid flow driven by buoyancy in a square enclosure with diverse fin heights, *Physics of Fluids*, 35, 2023, 122003.

[12] Varun Kumar, R.S., Chandan, K., Venkadeshwaran, K., Muhammad, T., Punith Gowda, R.J., Prasannakumara, B.C., Influence of magnetic dipole on the hybrid nanofluid flow with chemical reactions due to the generated and absorbed heat, *Pramana*, 99, 2025, 65.

[13] Sharma, R.P., Barik, B.K., Kumar, V.V., Sharma, A., Illustration of low oscillating magnetic field on sodium alginate-based hybrid nanofluid flow between two revolving disks: an artificial neural network-based study, *Engineering Applications of Artificial Intelligence*, 155, 2025, 111101.

[14] Pattnaik, P.K., Shamshuddin, M., Panda, S., Mishra, S.R., Eid, M.R., Modified Adomian decomposition mechanism for hybrid nanofluid flow through rocket engine nozzle based CoFe2O4 and Ag nanoparticles, *Chaos, Solitons & Fractals*, 197, 2025, 116521.

[15] Sharma, B., Srivastava, N., Fluid flow past a rotating sphere in the presence of a toroidal magnetic field, *ZAMM – Journal of Applied Mathematics and Mechanics*, 103, 2022, e202200218.

[16] Maurya, P.K., Deo, S., Maurya, D.K., Couple stress fluid flow enclosing a solid sphere in a porous medium: Effect of magnetic field, *Physics of Fluids*, 35, 2023, 072006.

[17] Sharma, R.P., Praharaj, S., Barik, B.K., Kumar, V.V., Sharma, A., Mahanta, C., Neural network-based analysis of thermal and mass transfer in nanofluid flow through a microchannel under pollutant concentration effect, *Multiscale and Multidisciplinary Modeling, Experiments and Design*, 8, 2024, 313.

[18] Kumar, A., Rajeev, Gómez-Aguilar, J.F., A numerical solution of a non-classical Stefan problem with space-dependent thermal conductivity, variable latent heat and Robin boundary condition, *Journal of Thermal Analysis and Calorimetry*, 147, 2022, 14649–14657.

[19] Dolui, S., Bhaumik, B., De, S., Combined effect of induced magnetic field and thermal radiation on ternary hybrid nanofluid flow through an inclined catheterized artery with multiple stenosis, *Chemical Physics Letters*, 811, 2022, 140209.

[20] Raza, Q., Wang, X., Mushtaq, T., Ali, B., Shah, N.A., Finite element analysis of copper nanoparticles in Boger fluid: Effects of dynamic inter-particle spacing, nanolayer thermal conductivity, nanoparticles diameter, and thermal radiation over a stretching sheet, *Chinese Physics B*, 2025, https://doi.org/10.1088/1674-1056/addcbc.

[21] Kumar, V.V., Sharma, R.P., Kumar, R.N., The role of time-varying nanofluid flow and particle aggregation on the kinetics of homogeneous and heterogeneous reactions in position-controlled squeezing porous slider, *Proceedings of the Institution of Mechanical Engineers Part N: Journal of Nanomaterials, Nanoengineering and Nanosystems*, 2025, https://doi.org/10.1177/23977914251338162.

[22] Usafzai, W.K., Aly, E.H., Alshomrani, A.S., Ullah, M.Z., Multiple solutions for nanofluids flow and heat transfer in porous medium with velocity slip and temperature jump, *International Communications in Heat and Mass Transfer*, 131, 2022, 105831.

[23] Mubaraki, A.M., Nuruddeen, R.I., Gomez-Aguilar, J.F., Closed-form asymptotic solution for the transport of chlorine concentration in composite pipes, *Physica Scripta*, 99, 2024, 075201.

[24] Farooq, U., Irfan, M., Khalid, S., Jan, A., Hussain, M., Computational convection analysis of second-grade MHD nanofluid flow through porous medium across a stretching surface, *ZAMM – Journal of Applied Mathematics and Mechanics*, 104, 2024, e202300401.

[25] Kumar, V.V., Sharma, R.P., Entropy generation minimization in nuclear reactor cooling via rough rotating disk: a statistical approach, *Multiscale and Multidisciplinary Modeling, Experiments and Design*, 8, 2025, 245.

[26] Raza, Q., Wang, X., Analyzing heat transfer behavior in two-dimensional Darcy–Forchheimer porous medium using magnetized nanoparticles, *Numerical Heat Transfer, Part B: Fundamentals*, 2024, 1–21, https://doi.org/10.1080/10407790.2024.2380034.
[27] Venkateswarlu, B., Chavan, S., Joo, S.W., Kim, S.C., Entropy analysis in squeezing flow of CoFe2O4+TiO2+MgO/H2O trihybrid nanofluid between parallel plates with viscous dissipation and chemical reaction: a numerical approach, *Numerical Heat Transfer, Part A: Applications*, 2024, 1–30, https://doi.org/10.1080/10407782.2024.2375634.
[28] Jagadha, S., Gopal, D., Patil, N., Singh, S., Kishan, N., Abhilasha, S.K., Effect of higher order chemical reaction and Joule heating on rotational and permeable radiative MHD flow of Casson manganese ferrite fluid with heat generation/absorption, *Multiscale and Multidisciplinary Modeling, Experiments and Design*, 8, 2025, 164.
[29] Sharma, A., Sharma, R.P., Exploring the impact of nanoparticle aggregation in parabolic trough solar collectors with neural network-based predictions for enhanced thermal performance, *Solar Energy Materials and Solar Cells*, 293, 2025, 113866.
[30] Gowtham, K.J., Gireesha, B.J., Pavithra, C.G., Investigation of Third-Grade fluid flow in an inclined microchannel: utilizing the Hermite wavelet technique for second law analysis, *Chemical Engineering Science*, 300, 2024, 120646.
[31] Madhu, J., Vinutha, K., Kumar, R.N., Gowda, R.J.P., Prasannakumara, B.C., Alqahtani, A.S., Malik, M.Y., Impact of solid–liquid interfacial layer in the nanofluid flow between stretching stationary disk and a rotating cone, *Tribology International*, 192, 2024, 109187.
[32] Soumya, D.O., Venkatesh, P., Srilatha, P., Chohan, J.S., Prasannakumara, B.C., Alshehri, M., Shah, N.A., Significance of TiO2–water nanofluid, buoyant strength and ohmic heating in the enhancement of microchannel efficiency, *Case Studies in Thermal Engineering*, 60, 2024, 104605.
[33] Sharma, A., Sharma, R.P., Utilizing neural networks to illustrate the dynamics of viscous fluid flow over curved surface with homogeneous and heterogeneous reactions, *Engineering Applications of Artificial Intelligence*, 159, 2025, 111629.
[34] Shamshuddin, M., Panda, S., Salawu, S.O., Mishra, S.R., Patil, V.S., Analysis of Casson ternary nanofluid integration under various thermal physical impacts with Cattaneo–Christov model: exploring magnified heat transfer in stretchy surface, *International Journal of Hydrogen Energy*, 101, 2025, 450–460.
[35] Pattanaik, P.K., Shamshuddin, M., Panda, S., Mishra, S.R., Eid, M.R., Modified Adomian decomposition mechanism for hybrid nanofluid flow through rocket engine nozzle based CoFe2O4 and Ag nanoparticles, *Chaos, Solitons & Fractals*, 197, 2025, 116521.
[36] Galal, A.M., Mishra, S.R., Baithalu, R., Kallel, M., Panda, S., Chamkha, A.J., Ali, R., Afshar, S.R., Three-dimensional flow of nanofluid through a vertical channel considering KKL model: hydrothermal analysis via response surface methodology, *Journal of the Taiwan Institute of Chemical Engineers*, 168, 2025, 105931.
[37] Kumar, V.V., Sharma, R.P., Taguchi design approach for thermal enhancement in time-varying fluid injection of MXene bi-hybrid nanofluid-lubricated porous slider, *Physics of Fluids*, 37, 2025, 093128.
[38] Fatima, N., Ali, A., Das, S., Almubaddel, F.S., Bentalib, A., Orlova, T., Electromagnetic influences on fractional hemodynamics of trihybrid nanolayered nanoparticles in a diverging ciliated microtube: a machine learning-assisted analysis for biomedical applications, *Journal of Computational and Applied Mathematics*, 474, 2026, 116929.
[39] Malika, M., Sonawane, S.S., Application of RSM and ANN for the prediction and optimization of thermal conductivity ratio of water-based Fe2O3 coated SiC hybrid nanofluid, *International Communications in Heat and Mass Transfer*, 126, 2021, 105354.
[40] Rana, P., Gupta, S., Gupta, G., Unsteady nonlinear thermal convection flow of MWCNT–MgO/EG hybrid nanofluid in the stagnation-point region of a rotating sphere with quadratic thermal radiation: RSM for optimization, *International Communications in Heat and Mass Transfer*, 134, 2022, 106025.
[41] Sharma, R.P., Shaw, S., MHD Non-Newtonian Fluid Flow past a Stretching Sheet under the Influence of Non-linear Radiation and Viscous Dissipation, *Journal of Computational and Applied Mathematics*, 8(3), 2022, 949–961.
[42] Israr Ur Rehman, M., Chen, H., Hamid, A., Numerical investigation of Cattaneo–Christov double diffusion and mixed convection effects in non-Darcian Sutterby nanofluid using multi-objective optimization through RSM, *International Journal of Hydrogen Energy*, 100, 2025, 1219–1230.
[43] Sharma, A., Sharma, R.P., Statistical and numerical analysis of MHD nanofluid (TiO2/EG) flow on a nonlinear curved stretching surface with heat source: a RSM approach, *ZAMM – Journal of Applied Mathematics and Mechanics*, 105, 2025, e202400513.
[44] Khan, W.A., Pop, I., Boundary-layer flow of a nanofluid past a stretching sheet, *International Journal of Heat and Mass Transfer*, 53, 2010, 2477–2483.
[45] Devi, S.S.U., Devi, S.P.A., Numerical investigation of three-dimensional hybrid Cu–Al2O3/water nanofluid flow over a stretching sheet with effecting Lorentz force subject to Newtonian heating, *Canadian Journal of Physics*, 94, 2016, 490–496.
[46] Sharma, R.P., Shukla, S., Mishra, S.R., Pattnaik, P.K., Analyzing the influence of inertial drag on hybrid nanofluid flow past a stretching sheet with Mintsa and Gherasim models under convective boundary conditions, *Journal of Thermal Analysis and Calorimetry*, 149, 2024, 2727–2737.
[47] Abdelmalek, Z., Qureshi, M.Z.A., Bilal, S., Raza, Q., Sherif, E.S.M., A case study on morphological aspects of distinct magnetized 3D hybrid nanoparticles on fluid flow between two orthogonal rotating disks: an application of thermal energy systems, *Case Studies in Thermal Engineering*, 23, 2021, 100744.
[48] Raza, Q., Wang, X., Ali, B., Eldin, S.M., Yang, H., Siddique, I., Role of nanolayer on the dynamics of tri-hybrid nanofluid subject to gyrotactic microorganisms and nanoparticles morphology vis two porous disks, *Case Studies in Thermal Engineering*, 51, 2023, 103534.
[49] Sharma, A., Sharma, R.P., Enhancing heat transfer rate in hybrid nanofluid flow past a stretching sheet: a response surface methodology approach, *Arabian Journal for Science and Engineering*, 2025, https://doi.org/10.1007/s13369-025-10295-7.

ORCID iD

Rajat Srivastava https://orcid.org/0000-0000-1713-9357
Ram Prakash Sharma https://orcid.org/0000-0002-3359-1316

How to cite this article: Srivastava, R., Sharma R.P. Central Composite Design-Based Parametric Study of Magnetically Dissipative Darcy–Forchheimer Hybrid Nanofluid Flow over an Expanding Sheet, *J. Appl. Comput. Mech.*, 12(5), 2026, 1035-1046. https://doi.org/10.22055/jacm.2025.48830.5529